Journal of Hazardous Materials 191 (2011) 94–102

Contents lists available at ScienceDirect

Journal of Hazardous Materials

journal homepage: www.elsevier.com/locate/jhazmat

Enhancement effect of relative humidity on the formation and regional respiratory deposition of secondary organic aerosol

Kuo-Pin Yu[a,*], Chi-Chi Lin[b], Shang-Chun Yang[a], Ping Zhao[b]

[a] Institute of Environmental and Occupational Health Sciences, National Yang-Ming University, No. 155, Sec. 2, Linong Street, Taipei 11221, Taiwan, ROC
[b] Department of Civil and Environmental Engineering, National University of Kaohsiung, No. 700, Kaohsiung University Rd., Kaohsiung 81148, Taiwan, ROC

ARTICLE INFO

Article history:
Received 28 December 2010
Received in revised form 9 April 2011
Accepted 12 April 2011
Available online 16 April 2011

Keywords:
Nanoparticles
Environmental chamber
d-Limonene
Ozone
Wall loss

ABSTRACT

In this study, we investigated the effect of relative humidity (RH) on the formation of secondary organic aerosol (SOA) generated from the ozonolysis of *d*-limonene in an environmental chamber. The mass yield and the number concentration of SOA increased seven and eight times, respectively, when the RH increased from 18% to 82%. The measured total loss rates (apparent loss rates) of the number and mass concentration of SOA in the chamber ranged from 1.70 to 1.77 h^{-1} and from 2.51 to 2.61 h^{-1}, respectively, at a controlled ventilation rate of $0.72 \pm 0.04\ h^{-1}$. The wall-deposition-loss-rate coefficient observed ($1.00 \pm 0.02\ h^{-1}$) was approximate to the estimated value based on Zhao and Wu's model [1] which includes the factors of turbulence, Brownian diffusion, turbophoresis and surface roughness. According to the ICRP (International Commission on Radiological Protection) model, the inhaled SOA particles are deposited primarily in the alveoli of the lung. The integrated alveolar deposited dose of the mass (surface area) of SOA over 3 h accounted for 74.0–74.8% (74.3–74.9%) of the total deposited dose at the investigated RH. Raising the RH resulted in the growth of SOA particle sizes and increment of the deposition dose but did not cause significant changes in the ratio of regional to the total respiratory deposition of SOA.

1. Introduction

Various so-called "natural" or "green" household products, making up detergents, air fresheners, paints and essential oils, etc. are more and more prevalent nowadays. However, they may contain plant extracts and biogenic volatile organic compounds (BVOCs) such as terpenoids [2–4]. The increasing use of such products has raised the indoor BVOCs concentrations [2]. *d*-Limonene (one kind of terpenoid), for example, is found in detergents, fragrances and some other consumer products and has been detected in indoor air at concentrations of 0.05–13 ppb [5]. The peak concentration of *d*-limonene can reach above 500 ppb during cleaning [6,7]. Moreover, some wooden materials and regular non-"green" consumer products used indoors may emit significant amounts of terpenoids as well [4,8,9]. Most BVOCs contain carbon–carbon double bonds and can be oxidized by reactive oxidative species, such as ozone and hydroxyl radicals. The oxidation of BVOCs by ozone can produce many non- and semi-volatile products which can partition into the particle phase rapidly and generate secondary organic aerosols (SOAs) [9–18].

The SOA particles formed via self-nucleation are ultrafine or nanoscale. Nanoparticles may cause harmful effects to human health because they can penetrate into the alveoli of the lung with subsequent translocation into blood and then reach other organs via systemic circulation [19–22]. The inhaled nanoparticles can also infiltrate into the central nervous system via the neuronal translocation through the olfactory nerves [19]. However, the negative health effects of the inhaled particulate matters are dependent on the regions of the respiratory tract that the particles are deposited in and the deposition dose. The regional deposition of aerosol particles in the respiratory tract depends on particle sizes, breathing pattern and respiratory condition (asthma, etc.). The particle sizes of SOA are affected significantly by the relative humidity (RH) owing to the hygroscopicity of SOA [23,24], the aqueous chemistry occurring on the surface of SOA [25–28], and the gas-phase reactions involving water [29]. In this study, we investigated the effects of RH on the formation, kinetic parameters and respiratory deposition of SOA generated from the ozonolysis of *d*-limonene.

2. Experimental

2.1. Experimental system

The experiments were conducted in a polished stainless steel chamber (60 cm × 60 cm × 60 cm) under a controlled ventilation

* Corresponding author. Tel.: +886 2 28267933; fax: +886 2 28278254.
E-mail addresses: kpyu@ym.edu.tw, f89541105@gmail.com (K.-P. Yu).

0304-3894/$ – see front matter © 2011 Elsevier B.V. All rights reserved.
doi:10.1016/j.jhazmat.2011.04.042

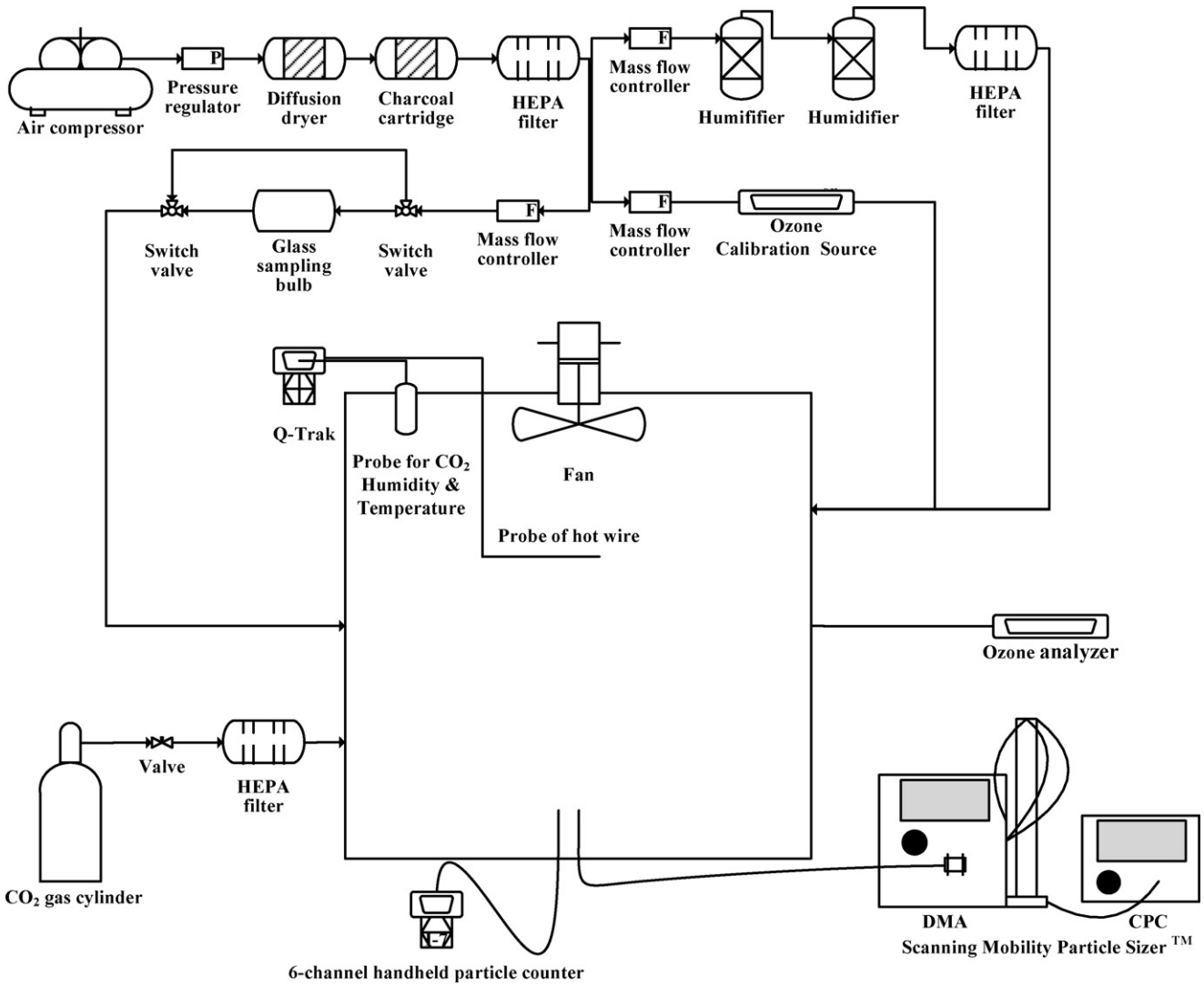

Fig. 1. Experimental system.

rate ($0.72 \pm 0.04\,h^{-1}$) and three controlled RH ($18 \pm 2\%$, $50 \pm 3\%$ and $82 \pm 2\%$) (see Fig. 1). The temperature of the experimental system was maintained at $23 \pm 2\,^{\circ}C$, which was controlled by the air-conditioning system of the lab. The supply air for the experimental system was provided by an oil-free air compressor (ORSO) equipped with a pressure regulator (AW300-02B, SMC, Japan). The humidity, organic vapors and particulate matters in the compressed air were removed by a homemade diffusion dryer packed with active aluminum oxide, a homemade charcoal cartridge and a HEPA filter (HEPA capsule, Part Number 12144, PALL Corporation, USA), respectively. The RH of the supply air was controlled by adjusting the ratio of the saturated-air flow rate to the dry-air flow rate. The water-vapor-saturated air was generated by passing the air through two homemade humidifiers connected in series. A HEPA filter (HEPA capsule) was installed at the outlet of the humidifier to eliminate water droplets. The flow rates of the dry air and saturated air were controlled by two mass flow controllers (Type 8711, Bürkert, Germany, deviation of flow rate <1.1%). A metal fan was located on the ceiling of the chamber to mix the chamber air. The temperature, RH and freestream air velocity inside the chamber were measured continuously by an indoor air quality monitor (Q-Trak 7565-X with a 962 probe and a 982 probe, TSI Inc., USA). Ozone produced by an Ozone Calibration Source™ (Model 306, 2B Technologies, USA) was introduced into the chamber continuously throughout the experiments. The ozone concentration in the chamber was monitored continuously by an ozone analyzer (Model 205, 2B Technologies, USA). The particle concentration and size distribution of the aerosols in the chamber was measured continuously by a Scanning Mobility Particle Sizer™ (SMPS, Model 3936L76, TSI Inc., USA) which gives the electrical mobility particle diameters. The length of the SMPS sampling tube was 50 cm. A 6-channel (0.3 μm, 0.5 μm, 1.0 μm, 2.5 μm, 5.0 μm and 10.0 μm) handheld particle counter (HANDHELD 3016 IAQ, LIGHTHOUSE, USA) was used simultaneously for the measuring of the concentration of larger particles (particle diameter >300 nm).

2.2. Experimental procedure

In each experiment, it took about 4 h to condition the chamber air. The experiments were carried out after the RH and ozone concentration (100 ± 5 ppb) of the chamber air achieved a steady state. Before each experiment, 0.5 μL of *d*-limonene liquid (purity of 99.3%, Lot: 408-120A, CHEM SERVICE, PA, USA) was injected into a 250-mL glass sampling bulb (SUPELCO, USA), and after the liquid completely evaporated (about 40 min after the injection), the valve used to direct the supply air flow was switched to the glass sampling bulb to introduce the *d*-limonene vapor into the chamber. The initial *d*-limonene concentration in the chamber was

1.94 ± 0.08 mg/m^3 as measured by the method described in our previous studies [30–34]. Before the *d*-limonene vapor was introduced into the chamber, a certain amount of CO_2 gas was injected into the chamber to serve as a tracer gas (CO_2 gas cylinder was purchased from C.C. Gaseous Corporation, Taiwan). By monitoring the change of the CO_2 concentration in the chamber, we obtained the target ventilation rate and mixing level and the methods for the estimation of ventilation rate and air mixing level were described in our previous study [33]. The mixing level of the chamber air was higher than 98%. The control experiments were conducted in the presence of *d*-limonene and CO_2 tracer while ozone was absent in the chamber. Between each two experiments, the chamber wall was cleaned with methanol and distilled water to remove the deposited SOA and organic compounds. Before each experiment, the chamber was purged with zero air at an air flow rate of 10 L/min for 4 h to eliminate residual organic compounds and particles. The gas sampling bulb was purged with heated zero air at an air flow rate of 2.5 L/min for 2 h to remove residual *d*-limonene. To verify that our experimental data were stable and reliable, each experiment was repeated more than three times. The coefficients of variation of the experimental data of SOA mass and number concentrations reported in this study are less than 0.1.

3. Results and discussion

3.1. Bimodal particle size distribution of SOA

We conducted the experiments under three different RH: 18 ± 2%, 50 ± 3% and 82 ± 2%, which represented the dry, moderate and humid conditions, respectively. As shown in Fig. 2(a)–(c), a burst of SOA with bimodal particle size distribution (main and minor branches) formed immediately after *d*-limonene was introduced into the chamber. The result of the control experiments showed that only trace particles (average concentration <20 particles/cm^3) appeared in the chamber before the introduction of *d*-limonene and no particle was introduced into the chamber along with *d*-limonene vapor and CO_2 tracer gas. The 'banana" growth curves shown in Fig. 2 clearly suggest the nucleation and new particle growth in the experiments. There is a possibility that some particles with very small sizes were introduced into the chamber along with *d*-limonene and CO_2 tracer gas when we switched the valve. However, due to the detection limit of the SMPS system (10 particles/cm^3 in concentration and 10 nm in particle diameter), this suspicion could not be verified so far.

The lognormal distribution fit parameters (number concentration, geometric median diameter and geometric standard deviation) of the main and minor branches of the SOA bursts for the first 2 h of our experiments are listed in Table 1. The bimodal particle size distribution of SOA might result from the self-nucleation of first- vs. second-generation products of the ozonolysis of *d*-limonene [9,35,36]. The main branch of the SOA burst might be formed from the first-generation products, partitioning into the particle phase via self-nucleation. The second-generation products were less volatile and formed more slowly than the first-generation ones (only a small amount of second-generation products formed at the beginning of the experiment). However, compared with the first-generation products, the second-generation products had a higher tendency to partition into particle phase via self-nucleation and could form smaller nuclei. These nuclei might grow up to be the minor branch of the SOA burst.

As shown in Table 1, the original particle diameter decreased with increasing RH but the particle number increased with the increase of RH. This phenomenon might result from the gas-phase reactions of the increasing water with the excited Criegee intermediates which produced more low volatility products [29].

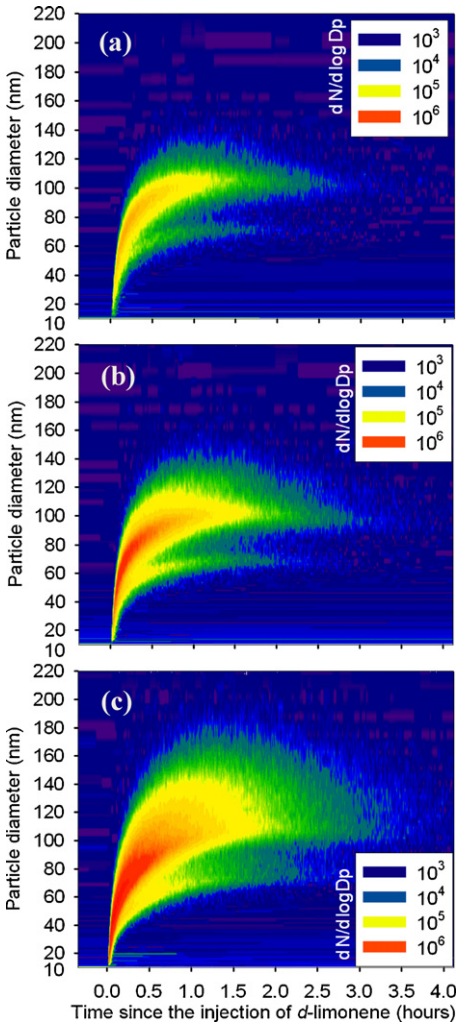

Fig. 2. Contour plots of SOA bursts formed under (a) RH 18%, (b) RH 50% and (c) RH 82%.

Conclusively, these low volatility products could form SOA particles with lower particle diameter and higher particle number via self-nucleation.

3.2. The deposition loss rate of particles to the wall

As shown in Fig. 3(a), the apparent loss rates of aerosol number concentrations in the chamber under various RH ranged from 1.70 to 1.77 h^{-1}. The decay of aerosol number may be due to the ventilation (0.72 ± 0.04 h^{-1}) and the deposition of aerosol particle on the chamber wall. A model developed by Lai and Nazaroff [37] has been applied to estimate the loss-rate coefficient, β, for particle deposition on the chamber wall in a previous study [9]. However, the deposition loss-rate coefficient estimated by this model, which focuses on the turbulent (eddy) and Brownian diffusion, is a particle-size-dependent coefficient, while the apparent loss rate of the total number concentration observed in this study did not change with the growth of particle size in the particle size region scanned (10–310 nm). Therefore, other transport mechanisms such as turbophoresis and the surface roughness may also play an important role in the deposition of SOA [1,38]. The deposition loss-rate coefficient estimated by Zhao and Wu's model [37] with a friction velocity of 4.8 cm/s and mean surface roughness height of 1 (dimensionless unit) is close to the overall deposition loss-rate coefficients observed in this study (1.00 ± 0.02 h^{-1}).

Table 1
SOA size distribution fit parameters.

RH	Time (h)	Minor branch (lognormal)			Main branch (lognormal)		
		N[a] (particle/cm^3)	GMD[b] (nm)	GSD[c]	N[a] (particle/cm^3)	GMD[b] (nm)	GSD[c]
82%	0.25	28,983	48	1.06	657,120	72	1.15
	0.5	20,940	58	1.06	353,560	89	1.16
	0.75	15,527	65	1.06	212,720	102	1.17
	1	13,371	69	1.07	138,680	108	1.17
	1.25	10,041	73	1.09	91,419	115	1.16
	1.5	5967	74	1.07	63,653	116	1.17
	1.75	3097	74	1.06	40,548	117	1.18
	2	2667	75	1.09	28,638	119	1.17
50%	0.25	56,786	55	1.14	273,200	76	1.11
	0.5	30,752	62	1.12	155,340	88	1.11
	0.75	16,383	65	1.07	95,581	95	1.11
	1	10,262	67	1.08	65,535	100	1.11
	1.25	7463	70	1.10	39,509	103	1.10
	1.5	4275	68	1.08	26,280	102	1.10
	1.75	3062	69	1.08	16,673	104	1.10
	2	2389	69	1.10	12,054	102	1.10
18%	0.25	27,975	60	1.13	117,420	79	1.09
	0.5	7935	62	1.08	90,252	92	1.09
	0.75	6941	66	1.09	52,877	100	1.08
	1	4182	70	1.08	26,870	102	1.09
	1.25	3690	70	1.08	16,794	104	1.08
	1.5	2341	70	1.09	12,610	105	1.08
	1.75	1375	71	1.06	9801	104	1.09
	2	845	72	1.04	4426	104	1.08

[a] Number concentration.
[b] Geometric median diameter.
[c] Geometric standard deviation.

The friction velocity (4.8 cm/s) was calculated based on Lai and Nazaroff's method [37] through the freestream air velocity (0.7 m/s) in the chamber.

3.3. Coagulation of SOA

Owing to the coagulation of the aerosol particles, the decay rates of particle number concentration were higher than the apparent loss rates when the concentrations were higher than 10^5 particles/cm^3. We assumed that the decay rate of particle number concentration resulted from the coagulation can be described by the classical Brownian coagulation model with "an apparent coagulation coefficient" for the overall particle number (the model is as the same as the coagulation of monodispersed aerosol in mathematics but is different in concept), and the overall decay rate of particle number concentration in the chamber air can be expressed as what follows:

$$\frac{dN}{dt} = -KN^2 - kN \tag{1}$$

where N is the number concentration of aerosol particles; t is the time elapsed; K is the apparent coagulation coefficient; k is the apparent loss rate of the particle number concentration shown in Fig. 3(a). The apparent coagulation coefficient of aerosol particle was used to simplify the coagulation model. Rearranging Eq. (1) and then integrating the resulting equation in the interval $t = 0$ to t and $N = N_0$ to $N(t)$, we have:

$$\frac{1}{k} \ln\left[\frac{N_0/(k + KN_0)}{N(t)/(k + KN(t))}\right] = t \tag{2}$$

Rearranging the equation above, we have:

$$k\left[\exp(kt) \times \frac{N(t)}{N_0} - 1\right] = KN(t)[1 - \exp(kt)] \tag{3}$$

According to Eq. (3), the plot of $k[\exp(kt)N(t)/N_0 - 1]$ vs. $N(t)[1 - \exp(kt)]$ should be linear with a slope equal to the apparent coagulation coefficient. These linear relationships are illustrated in Fig. 4(a), and the apparent coagulation coefficients in the cases of RH 82% and RH 50% are $3.8 \pm 0.2 \times 10^{-6}$ and $3.5 \pm 0.2 \times 10^{-6}$ cm^3/particle-h ($1.05 \pm 0.05 \times 10^{-9}$ and $9.72 \pm 0.42 \times 10^{-10}$ cm^3/particle-s), respectively. The apparent coagulation coefficients obtained in this study are similar but a little larger than that given by Lee and Chen [39] for aerosols with lognormal distribution of particle sizes. The enlargement of coagulation coefficient might be owing to the bimodal lognormal particle size distribution of SOA at the beginning of the experiment, since the broader particle size distribution (bimodal lognormal as compared to single lognormal) could result in larger coagulation coefficients.

3.4. Kinetics model

For the simplicity of the kinetics model, we assumed that the complicated process of the SOA formation and loss can be simplified as the following steps:

$$O_3 + d\text{-limonene} \xrightarrow{k_1} y\text{SOA} \tag{4}$$

$$d\text{-limonene} \xrightarrow{\lambda} \text{vent} \tag{5}$$

$$\text{SOA} \xrightarrow{k_2} \text{wall} \tag{6}$$

$$\text{SOA} \xrightarrow{\lambda} \text{vent} \tag{7}$$

where y is the mass yield of SOA resulting from the ozonolysis of d-limonene; k_1 is the reaction rate coefficient of ozonolysis of d-limonene; k_2 is the decay constant of SOA resulting from the wall loss; λ is the ventilation rate of the chamber. Thus, the time evolution of d-limonene and SOA concentrations can be written as:

$$\frac{d[d\text{-limonene}]}{dt} = -k_1[O_3][d\text{-limonene}] - \lambda[d\text{-limonene}] \tag{8}$$

$$\frac{d[\text{SOA}]}{dt} = k_1 y[O_3][d\text{-limonene}] - (k_2 + \lambda)[\text{SOA}] \tag{9}$$

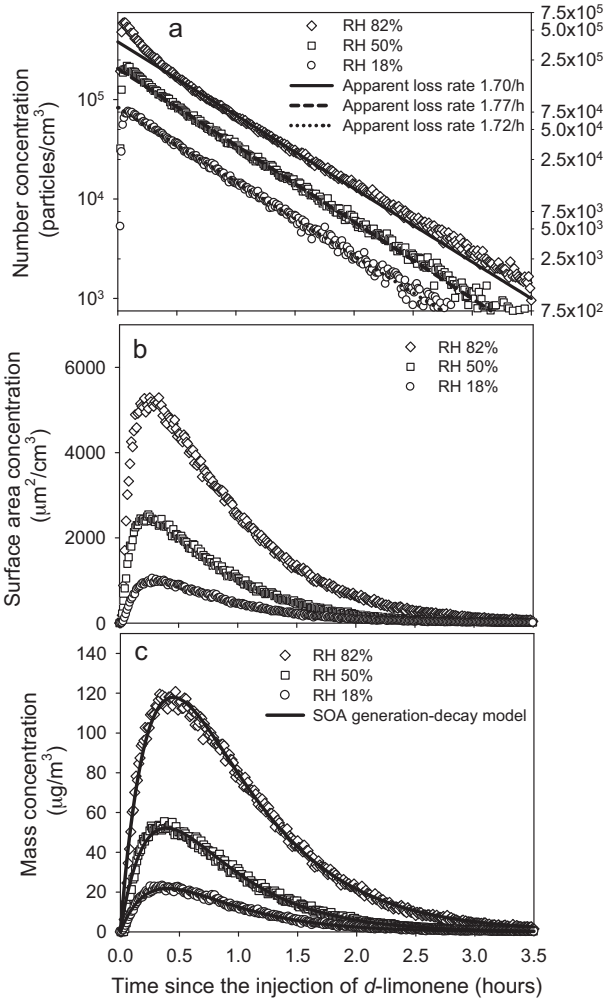

Fig. 3. (a) Number, (b) surface area and (c) mass concentrations of the SOA bursts formed under RH 82% (ACH = 0.72 h^{-1}), RH 50% (ACH = 0.75 h^{-1}) and RH 18% (ACH = 0.74 h^{-1}). The density of particle was assumed to be 1.6 kg/m^3 [40]. The density of SOA generating from the ozonolysis of *d*-limonene has been reported to be 1.21–1.65 g/cm^3 [18,40]. The hygroscopic growth of SOA could result in the decrease of density, but the partitioning of small aldehydes, ketones and alcohols in the gas phase into the wet surface and the sequent reactions with ozone and hydroxyl radical would probably increase the density. However, due to the lack of data, we assume the same density of SOA under various RH.

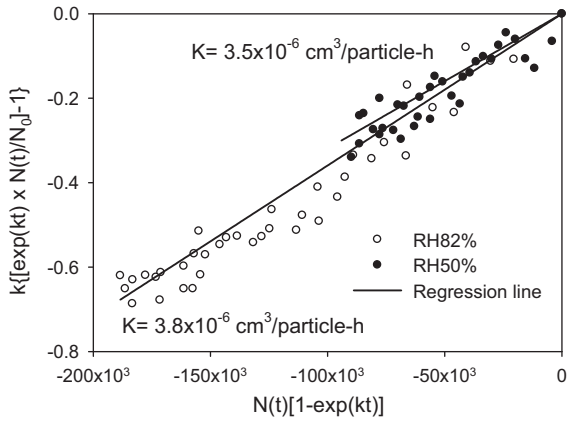

Fig. 4. Plots of $k\{[\exp(kt)N(t)/N_0] - 1\}$ vs. $N(t)[1 - \exp(kt)]$ for RH 82% ($t < 0.6$ h) and RH 50% ($t < 0.4$ h).

Table 2
Mass yield and decay constant retrieved from the regression of SOA generation-decay model.

	Mass yield, y	Decay constant, k_2
RH 18%	0.070 ± 0.007	2.53 ± 0.21 h^{-1}
RH 50%	0.174 ± 0.013	2.61 ± 0.20 h^{-1}
RH 82%	0.534 ± 0.019	2.51 ± 0.15 h^{-1}

where [*X*] is the mass concentration of species *X* (μg/m^3). When the ozone concentration is at a steady state, Eqs. (8) and (9) can be rewritten as Eqs. (10) and (11), respectively:

$$\frac{d[d\text{-limonene}]}{dt} = -k_1'[d\text{-limonene}] \quad (10)$$

$$\frac{d[\text{SOA}]}{dt} = (k_1' - \lambda)y[d\text{-limonene}] - (k_2 + \lambda)[\text{SOA}] \quad (11)$$

in which $k_1' = k_1[O_3] + \lambda$.

There was no *d*-limonene and SOA in the supply air (zero air) and the initial concentrations of *d*-limonene and SOA were $[d\text{-limonene}]_0$ and zero, respectively. Thus, the analytical solution of Eq. (10) is:

$$[d\text{-limonene}] = [d\text{-limonene}]_0 \exp(-k_1' t) \quad (12)$$

Substituting Eq. (12) into Eq. (11) and solving the resulting differential equation, we have:

$$[\text{SOA}] = \frac{(k_1' - \lambda)y[d\text{-limonene}]_0}{k_2 + \lambda - k_1'}\{\exp(-k_1' t) - \exp[-(k_2 + \lambda)t]\} \quad (13)$$

We used Eq. (13), which was named as the SOA generation-decay model, to fit our experimental data, as demonstrated in Fig. 3(c). The parameters retrieved from the fitting curves are listed in Table 2. The surface area and the mass of the particles were calculated based on the assumption that the particles are spherical and with a density of 1.6 g/cm^3 [40]. It is note that the PM2.5 contributed by only the SOA could exceed the acceptable standards of air quality (100 mg/m^3: the guideline value of indoor PM2.5 proposed by the Environmental Protection Administration of Taiwan). There is a high possibility that the SOA could partition into the preexisting aerosol particles (seeds) and worsen the air quality especially under higher RH. High RH in indoor environments is very common in many tropical and subtropical countries.

The semi-volatile products generated from the ozonolysis of *d*-limonene may also lose due to the deposition to the chamber wall and ventilation. However, the loss rate of the semi-volatile products resulting from the deposition to the wall and ventilation was much less than that of condensation on the SOA surface. The first-order decay rate for the deposition of the condensable vapors to the chamber wall is 3.45 h^{-1}, which was estimated by Lai and Nazaroff model [37] through the friction velocity of 0.07 m/s and a plausible diffusion coefficient of the *d*-limonene vapor of 0.0803 cm^2/s. (The diffusion coefficient of the semi-volatile products of *d*-limonene ozonolysis should be lower.) The mass transfer rate coefficient (m_g) for the condensation of the semi-volatile products of *d*-limonene ozonolysis on the SOA surface could be estimated by using the Fuchs theory of mass transfer of a gas molecule to a particle in the transition regime [41]:

$$m_g = 2\pi D_p D_g \beta_F \quad (14)$$

in which D_g is the diffusion coefficient of the semi-volatile products (assumed as 0.04 cm^2/s); D_p is the particle diameter; β_F is the correction factor, which ranges from 0.7 to 1. The first-order decay rate

for the condensation of semi-volatile products to the SOA surface was calculated using Eq. (15) at each particle scan data:

$$\int_{D_{p\,\min}}^{D_{p\,\max}} m_g \left(\frac{dN}{d\log dD_p}\right) d\log dD_p \quad (15)$$

The first-order decay rate for the condensation just after the initial nucleation was 712 h^{-1} under RH 18% and achieved a maximum of 13,135 h^{-1} few minutes later. Over the ranges of particle diameters and vapor diffusivities, the mass transfer rate of semi-volatile products on the SOA surface was at least two orders of magnitude faster than that of vapor deposition onto chamber wall and ventilation.

3.5. Enhancement effect of humidity on mass and number of SOA

As shown in Table 2, the mass yield of SOA increased from 0.070 ± 0.007 to 0.534 ± 0.019, when the RH increased from 18% to 82%. Both the number and mass concentrations of SOA increased with the increase of RH, as shown in Fig. 3(a) and (c). Hygroscopic growth of SOA could partially explain the increase of the mass of SOA. The water molecules can be adsorbed on the hydrophilic functional group (e.g., hydroxyl (–OH), carboxylic (–COOH), ketone (>CO), and aldehyde (–HCO)) born by the polar oxygenated compounds on the surface of SOA [24]. However, Jonsson et al. [29] suggested that the physical water up-take contributed only, at a maximum, 30% of the increase of the SOA volume. They concluded that the increase of water concentration could enhance the gas-phase reactions of water with the excited Criegee intermediates and produce more low volatility products, which could form SOA through self-nucleation and condensation. For example, the energy-rich Criegee biradicals can be collisionally stabilized by air and water molecules and then transform to carboxylic acid by reacting with water molecules [41]. Nevertheless, while our experiments were conducted in a chamber system, the experiments of Jonsson et al. [29] were carried out in a flow-tube system, in which the retention time of the *d*-limonene and ozone was only 4.5 min (268–272 s) and the reaction of *d*-limonene ozonolysis in Jonsson's experiments might not be complete. As a result, in our experiments the SOA mass and number increased six times and eight times, respectively, when RH increased from 18% to 82%, while both of the SOA mass and number in Jonsson's experiments increased only about two times under similar RH condition.

Another explanation for the enhancement effect of humidity on mass and number of SOA is relevant to the atmospheric processes involving SOA formation through aqueous chemistry in clouds and wet aerosols [25–28]. In this process, small aldehydes, ketones and alcohols generated from the ozonolysis of *d*-limonene in the gas phase can partition into the wet surface of the hygroscopic SOA at high RH. These small aldehydes, ketones and alcohols hydrate and react further with ozone or hydroxyl radical (hydroxyl radical is a by-product of the ozonolysis of *d*-limonene [42]) on the wet surface of SOA and generate low-volatility products [28]. However, these small aldehydes, ketones and alcohols would not form SOA through vapor-particle partitioning at low RH. In addition, this process may not be observed in a flow-tube system (e.g. Jonsson et al. [29]) in which the retention time is too short to complete the process.

3.6. Respiratory deposition and health effects of SOA

The predicted regional respiratory deposited dose of SOA based on ICRP (International Commission on Radiological Protection) model for human beings [43], which was calculated by the following equation, is shown in Fig. 4:

$$\text{Deposited dose} = [\text{SOA}] \times \text{DF} \times \text{BR} \quad (16)$$

in which [SOA] is the mass or surface area concentrations of SOA; DF is the deposition fraction of particulate matters in nasal passage and pharynx (nasopharyngolaryngeal deposition), trachea, bronchus and bronchioles (tracheobronchial deposition), and the alveoli of the lung (alveolar deposition) during nose breathing; BR is the breathing rate assumed (1.2 m^3/h, 20 L/min). This breathing rate is a little lower than that during the light exercise (light exercise mode) in the ICRP model and higher than that at rest (sitting mode). This is a reasonable assumption and it can represent the breathing rate of a healthy adult under normal indoor activities.

Most of the air quality guidelines for aerosol particles are accessed on the basis of the mass concentrations of the particulate matter (e.g. National Ambient Air Quality Standards). However, the surface area of ultrafine particles or nanoparticles per given mass is much higher than that of larger particles (e.g. fine particles). Therefore, the responses such as pulmonary inflammation induced by ultrafine particles per given mass may be more serious than that induced by larger particles. For example, Oberdörster and his coworkers [44] found that the fumes of polytetrafluoroethylene (PTFE) with count median diameter of *ca.*18 nm and concentration of 50 μg/m^3 could induce serious pulmonary toxicity and lethality in rats after 15 min of exposure via inhalation. However, the agglomeration of these PTFE fumes would result in the loss of toxicity [44]. In the same study, Oberdörster's group dosed rats with ultrafine (25 nm) and fine (250 nm) TiO_2 particles and evaluated the inflammatory responses in their lungs after 24 h. They found the ultrafine TiO_2 particles would induce higher inflammatory responses than the fine TiO_2 particles per given mass. However, when they compensated for the surface area of these two different particle sizes, they got two virtually identical dose–response relationships. The concept of using the particle surface area as the appropriate dosing metric for the evaluation of the toxicity of particulate matter has been suggested by Donaldson et al. [45] and Oberdörster [46] and has been verified by Li et al. [47] by eliciting the inflammatory responses in the lung induced by carbon-black particles. Based on the reasons above, we present the deposited dose rates in terms of the surface area and mass of SOA in Fig. 5. As shown in Fig. 5, the maximum alveolar deposited dose rates of surface area of SOA under RH 18, 50 and 82% were 2.4, 6.6 and 15 cm^2/h, respectively, while the maximum alveolar deposited dose rates of mass of SOA were 4.8, 15 and 25 μg/h, respectively. The maximum deposited dose of SOA occurred between 6 and 15 min after the injection of *d*-limonene into the chamber and increased by increasing RH. Owing to the small sizes of SOA (<220 nm), they are deposited mainly in the alveoli of the lung. As illustrated in Fig. 6, the integrated alveolar deposited dose of the surface area and mass of SOA over 3 h contributed 74.1–74.9% of the total deposited dose. Based on epidemiologic and physiological research, exposure to particulate matters is associated with cardiopulmonary mortality, like pulmonary and systemic inflammation, accelerated atherosclerosis, and arrhythmia [48]. Three mechanisms may explain how ultrafine particles deposited in the lung induce these cardiopulmonary effects. The first hypothesis is that the ultrafine particles can stimulate the neurons in the lung and further affect the central nervous system and cardiovascular autonomic function. The second is the rapid translocation of the deposited ultrafine particles into the circulatory system. Once these particles reach the target organs through the systematic circulation, they may result in inflammation, excretions of cytokines, reactive oxygen species (ROS), C-reactive proteins (a kind of protein in the blood which is synthesized in the liver and excreted by the lipocyte), etc. and cause the cardiac events. The translocation of ultrafine particles from the lung into the blood circulation system in human bodies has been observed *in vivo* with ^{99m}Technetium-labeled ultrafine carbon particles [21]. However, the degree of extrapulmonary translocation depends on the size and surface chemistry of particles [49]. The

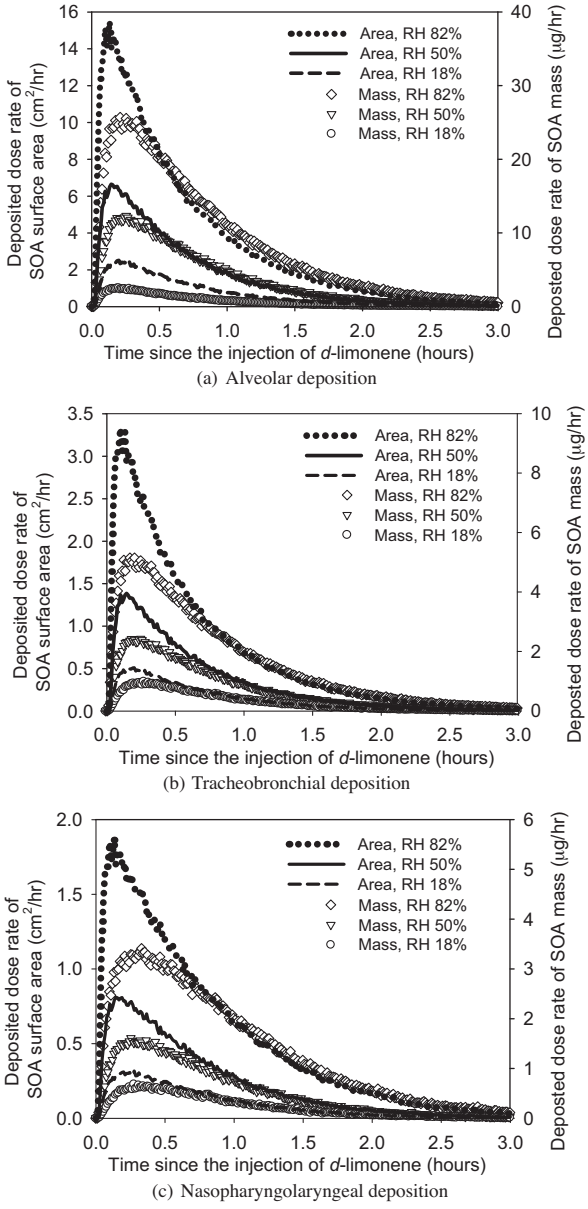

Fig. 5. (a) Alveolar (AL), (b) tracheobronchial (TB) and (c) nasopharyngolarygeal (NP) deposited dose of SOA surface area and mass under different RH.

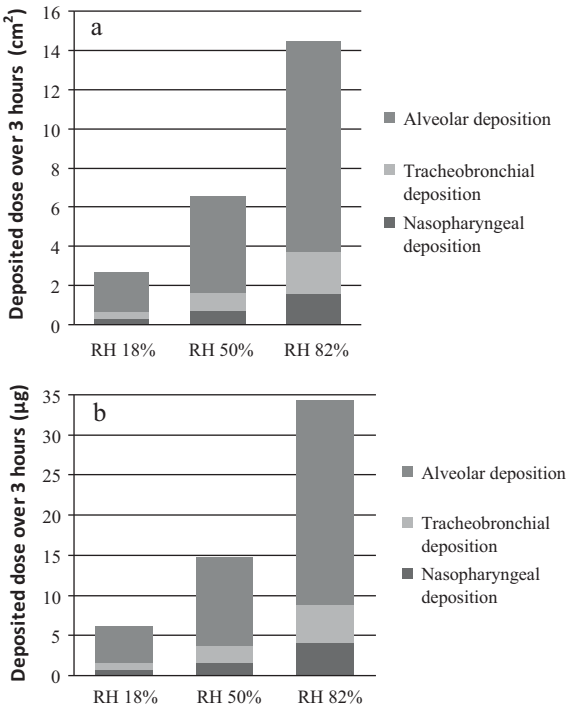

Fig. 6. Comparison of deposited dose of SOA (a) surface area and (b) mass over 3 h in different regions of respiratory system under various RH.

third hypothesis is that the deposited particles may induce acute inflammation in the lung, and as a result, stimulate the secretion of cytokines, chemokines, reactive oxygen species and transcription factor. The cascade of following events and inflammation is a key factor in the activation of the mitogen-activated protein kinase (MAPK), redox-sensitive transcription factor, nuclear factor κ B (NF-κB) and activating protein-1 (AP-1), and thus may worsen the inflammation of the lung that results in cardiac events [19].

The maximum nasopharyngolaryngeal deposited doses of mass (surface area) of SOA under RH 18%, 50% and 82% were 0.6 μg/h (0.3 cm^2/h), 1.8 μg/h (0.8 cm^2/h) and 3.4 μg/h (1.8 cm^2/h), respectively, while the maximum tracheobronchial deposited doses were 0.9 μg/h (0.5 cm^2/h), 3.0 μg/h (1.4 cm^2/h) and 5.1 μg/h (3.2 cm^2/h), correspondingly, as shown in Fig. 5(c) and (b). The tracheobronchial and nasopharyngolaryngeal deposition doses of SOA increased when RH increased. As demonstrated in Fig. 6(a) and (b), the tracheobronchial and nasopharyngolaryngeal deposition doses of mass (surface area) of SOA contributed 14.0–14.4% (14.5–14.7%) and 10.8–11.9% (10.5–11.1%) of the total deposition dose, respectively. Larger particles deposited on these two respiratory regions can be removed by the mechanism of mucociliary escalator [50]. However, some unique neuronal translocation pathways for ultrafine particles, which are relevant to the adverse health effects of ultrafine particles, have been demonstrated in rodents [51,52] and guinea pigs [53]. The olfactory axonal transportation of poliomyelitis virus particle (30 nm) with a transport velocity of 2.4 mm/h has been observed in chimpanzees [54]. Similar translation pathways that might be found in humans include uptake into the nerve endings of olfactory and trigeminal nerves which are implanted in nasal mucosa and the nerve endings of afferent vagal nerves which are embedded in tracheobronchial mucosa [49,52]. Translocation of ultrafine particles into the central nervous system can cause adverse health effects. For example, the oxidative stress (lipid peroxidation) induced by uncoated fullerenes (C_{60}) in the brain has been shown *in vivo* in juvenile largemouth bass [55]. However, the toxicity of ultrafine particles depends on their nature and chemical properties. For instance, the *d*-limonene ozonolysis reaction has been reported to produce a significant amount of reactive oxygen species (ROS) (ROS/SOA ratio is about 0.15–0.18 nmol/μg) which can partition into the SOA and penetrate deeply into the lung [18]. Therefore, the analysis of the chemical compositions of ultrafine particles is important for the assessment of their health effects.

An inhalation study conducted by McDonald and his coworkers demonstrated that only a mild response of the upregulation of heme oxygenase-1 and metalloproteinase-9 had been observed in mouse aorta when the mouse aorta was exposed to 200 mg/m^3 of SOA generated from the oxidation of α-pinene for 7 days [56]. Gaschen et al. [57] found that exposure to SOA with concentration of about 10^4 particles/cm^3 for 2 h caused only moderate responses of lung cells *in vitro*, and the cellular responses were related to the particle number concentration. A decrease in phagocytic activity was observed in human macrophages when being exposed to SOA generated from the ozonolysis of α-pinene. According to McDonald et al. [56] and Gaschen et al. [57], exposure to the SOA concentration observed in this study (~10^5 particles/cm^3 and ~100 μg/m^3)

would cause only mild or moderate responses of the lung cell. However, in another toxicological study, Jang and her coworkers exposed the BEAS-2B cell (bronchial epithelial cell) to SOA coated magnetic nanoparticles which were directed by a magnetic field to the target BEAS-2B cells [58]. They found a linear dose–response relationship between the mass of SOA delivered to the BEAS-2B cells and the proinflammatory mediator (interleukin-8) released by these cells. Consequently, the cellular response might be associated with the real dose that the cell was exposed to instead of the SOA concentration in the atmosphere. However, there are relatively few toxicological studies of SOA, and the evaluation of the responses caused by the respiratory deposited dose of SOA could be very difficult to implement based on the limited available information. Further relevant studies are needed to realize the potential health effects and dose–response relationship of exposure to SOA. Besides, the analysis of the chemical composition of SOA is significant for the evaluation of their health effect and will be our future work.

4. Conclusions

We investigated the effects of RH on the formation of SOA and their regional respiratory deposition based on chamber tests. In our experiments, a burst of SOA with a bimodal lognormal size distribution formed rapidly after *d*-limonene was introduced into the chamber and achieved a maximum mass concentration within 16 min. The bimodal size distribution might result from the nuclei of two different sizes formed via the self-nucleation of oxidized organic compounds with different volatilities.

In our experiments, the increase of RH leads to the increase in both the number and mass concentrations of SOA. The mechanisms involved in the enhancement effect of humidity on the SOA formation may include physical water uptake, the gas-phase reaction of water with the excited Criegee intermediates that produces more low-volatility products and SOA formation through aqueous chemistry.

The decay of the number concentration of SOA in the chamber is caused by the air exchange and wall loss. The mechanisms of wall loss may include turbophoresis, turbulence (eddy) and Brownian diffusion. The inhaled SOA would be deposited mainly (>74%) in the alveoli of the lung. Although the increase of RH resulted in the growth of the particle size of SOA, these changes did not cause significant changes in the ratio of regional to the total respiratory deposition dose of SOA.

The toxicity of ultrafine particles such as SOA depends on not only their dose but also their nature and chemical properties. Consequently, the detailed analysis of the chemical composition of SOA would help evaluate the health effects of SOA and will be important in our future works.

Acknowledgements

The authors would like to thank the National Science Council (NSC) of Republic of China for funding this research (under project contract number NSC 98-2218-E-010-003) and the grant from the Ministry of Education—Aim for the Top University Plan. We also wish to thank Ms. Jiayu Chen for the help of English editing.

References

[1] B. Zhao, J. Wu, Modeling particle deposition onto rough walls in ventilation duct, Atmospheric Environment 40 (2006) 6918–6927.
[2] C. Weschler, Changes in indoor pollutants since the 1950s, Atmospheric Environment 43 (2009) 153–169.
[3] H.-J. Su, C.-J. Chao, H.-Y. Chang, P.-C. Wu, The effects of evaporating essential oils on indoor air quality, Atmospheric Environment 41 (2007) 1230–1236.
[4] J. Toftum, S. Freund, T. Salthammer, C.J. Weschler, Secondary organic aerosols from ozone-initiated reactions with emissions from wood-based materials and a "green" paint, Atmospheric Environment 42 (2008) 7632–7640.
[5] L.C. Holcomb, B.S. Seabrook, Review: Indoor concentrations of volatile organic compounds: implications for comfort, health and regulation, Indoor and Built Environment 4 (1995) 7–26.
[6] A.C. Rohr, C.J. Weschler, P. Koutrakis, J.D. Spengler, Generation and quantification of ultrafine particles through terpene/ozone reaction in a chamber setting, Aerosol Science and Technology 37 (2003) 65–78.
[7] B.C. Singer, H. Destaillats, A.T. Hodgson, W.W. Nazaroff, Cleaning products and air fresheners: emissions and resulting concentrations of glycol ethers and terpenoids, Indoor Air 16 (2006) 179–191.
[8] W.W. Nazaroff, C.J. Weschler, Cleaning products and air fresheners: exposure to primary and secondary air pollutants, Atmospheric Environment 38 (2004) 2841–2865.
[9] B.K. Coleman, M.M. Lunden, H. Destaillats, W.W. Nazaroff, Secondary organic aerosol from ozone-initiated reactions with terpene-rich household products, Atmospheric Environment 42 (2008) 8234–8245.
[10] A. Alshawa, A.R. Russell, S.A. Nizkorodov, Kinetic analysis of competition between aerosol particle removal and generation by ionization air purifiers, Environmental Science & Technology 41 (2007) 2498–2504.
[11] G. Sarwar, R. Corsi, The effects of ozone/limonene reactions on indoor secondary organic aerosols, Atmospheric Environment 41 (2007) 959–973.
[12] T. Wainman, J. Zhang, C.J. Weschler, P.J. Lioy, Ozone and limonene in indoor air: a source of submicron particle exposure, Environmental Health Perspectives 108 (2000) 1139–1145.
[13] M.S. Waring, J.A. Siegel, R.L. Corsi, Ultrafine particle removal and generation by portable air cleaners, Atmospheric Environment 42 (2008) 5003–5014.
[14] C.J. Weschler, H.C. Shields, Indoor ozone/terpene reactions as a source of indoor particles, Atmospheric Environment 33 (1999) 2301–2312.
[15] C.J. Weschler, Ozone's impact on public health: contributions from indoor exposures to ozone and products of ozone-initiated chemistry, Environmental Health Perspectives 114 (2006) 1489–1496.
[16] C.J. Weschler, J.R. Wells, D. Poppendieck, H. Hubbard, T.A. Pearce, Workgroup report: indoor chemistry and health, Environmental Health Perspectives 114 (2006) 442–446.
[17] L. Morawska, C. He, G. Johnson, H. Guo, E. Uhde, G. Ayoko, Ultrafine particle in indoor air of a school: possible role of secondary organic aerosols, Environmental Science & Technology 43 (2009) 9103–9109.
[18] X. Chen, P.K. Hopke, A chamber study of secondary organic aerosol formation by limonene ozonolysis, Indoor Air 20 (2010) 320–328.
[19] M.R. Gwinn, V. Vallyathan, Nanoparticles: health effects—pros and cons, Environmental Health Perspectives 114 (2006) 1818–1825.
[20] G. Oberdörster, Z. Sharp, V. Atudorei, A. Elder, R. Gelein, A. Lunts, W. Kreyling, C. Cox, Extrapulmonary translocation of ultrafine carbon particles following whole-body inhalation exposure of rats, Journal of Toxicology and Environmental Health Part A 65 (2002) 1531–1543.
[21] A. Nemmar, P.H.M. Hoet, B. Vanquickenborne, D. Dinsdale, M. Thomeer, M.F. Hoylaerts, H. Vanbilloen, L. Mortelmans, B. Nemery, Passage of inhaled particles into the blood circulation in humans, Circulation 105 (2002) 411–414.
[22] A. Nemmar, H. Vanbilloen, M.F. Hoylaerts, P.H.M. Hoet, A. Verbruggen, B. Nemery, Passage of intratracheally instilled ultrafine particles from the lung into the systemic circulation in hamster, American Journal of Respiratory and Critical Care Medicine 164 (2001) 1665–1668.
[23] V. Varutbangkul, F.J. Brechtel, R. Bahreini, N.L. Ng, M.D. Keywood, J.H. Kroll, R.C. Flagan, J.H. Seinfeld, A. Lee, A.H. Goldstein, Hygroscopicity of secondary organic aerosols formed by oxidation of cycloalkenes, monoterpenes, sesquiterpenes, and related compounds, Atmospheric Chemistry and Physics 6 (2006) 2367–2388.
[24] M. Jaoui, E. Corse, T.E. Kleindienst, J.H. Offenberg, M. Lewandowski, E.O. Edney, Analysis of secondary organic aerosol compounds from the photooxidation of *d*-limonene in the presence of NO_x and their detection in ambient PM2.5, Environmental Science & Technology 40 (2006) 3819–3828.
[25] J.D. Blando, B.J. Turpin, Secondary organic aerosol formation in cloud and fog droplets: a literature evaluation of plausibility, Atmospheric Environment 34 (2000) 1623–1632.
[26] Y. Tan, A.G. Carlton, S.P. Seitzinger, B.J. Turpin, SOA from methylglyoxal in clouds and wet aerosols: measurement and prediction of key products, Atmospheric Environment 44 (2010) 5218–5226.
[27] Y.B. Lim, Y. Tan, M.J. Perri, S.P. Seitzinger, B.J. Turpin, Aqueous chemistry and its role in secondary organic aerosol (SOA) formation, Atmospheric Chemistry and Physics Discussions 10 (2010) 14161–14207.
[28] I. Grgić, L.I. Nieto-Gligorovski, S. Net, B. Temime-Roussel, S. Gligorovski, H. Wortham, Light induced multiphase chemistry of gas-phase ozone on aqueous pyruvic and oxalic acids, Physical Chemistry Chemical Physics 12 (2010) 698–707.
[29] Å.M. Jonsson, M. Hallquist, E. Ljungström, Impact of humidity on the ozone initiated oxidation of limonene, Δ3-carene, and α-pinene, Environmental Science & Technology 40 (2006) 188–194.
[30] K.-P. Yu, G.W.M. Lee, Decomposition of gas-phase toluene by the combination of ozone and photocatalytic oxidation process (TiO_2/UV, TiO_2/UV/O_3, and UV/O_3), Applied Catalysis B: Environmental 75 (2007) 29–38.
[31] K.-P. Yu, G.W.-M. Lee, C.-P. Hsieh, C.-C. Lin, Evaluation of ozone generation and indoor organic compounds removal by air cleaners based on chamber tests, Atmospheric Environment 45 (2011) 35–42.

[32] K.-P. Yu, G.W.-M. Lee, G.-H. Huang, The effect of ozone on the removal effectiveness of photocatalysis on indoor gaseous biogenic volatile organic compound, Journal of the Air & Waste Management Association 60 (2010) 820–829.
[33] K.-P. Yu, G.W.-M. Lee, W.-M. Huang, C.-C. Wu, C.-L. Lou, S. Yang, Effectiveness of photocatalytic filter for removing VOCs in heating ventilating and air-conditioning (HVAC) systems, Journal of Air and Waste Management Association 56 (2006) 666–674.
[34] K.-P. Yu, G.W.M. Lee, W.-M. Huang, C. Wu, S. Yang, The correlation between photocatalytic oxidation performance and chemical/physical properties of indoor volatile organic compounds, Atmospheric Environment 40 (2006) 375–385.
[35] N.L. Ng, J.H. Kroll, M.D. Keywood, R. Bahreini, V. Varutbangkul, R.C. Flagan, J.H. Seinfeld, A. Lee, A.H. Goldstein, Contribution of first-versus second-generation products to secondary organic aerosols formed in the oxidation of biogenic hydrocarbons, Environmental Science & Technology 40 (2006) 2283–2297.
[36] J.H. Kroll, J.H. Seinfeld, Chemistry of secondary organic aerosol: formation and evolution of low-volatility organics in the atmosphere, Atmospheric Environment 42 (2008) 3593–3624.
[37] A.C.K. Lai, W.W. Nazaroff, Modeling indoor particle deposition from turbulent flow onto smooth surfaces, Journal of Aerosol Science 31 (2000) 463–476.
[38] T. Hussein, L. Kubincová, L. Džumbová, A. Hruška, P. Dohányosová, J. Hemerka, J. Smolik, Deposition of aerosol particles on rough surfaces inside a test chamber, Building and Environment 44 (2009) 2056–2063.
[39] K. Lee, H. Chen, Coagulation rate of polydisperse particles, Aerosol Science and Technology 3 (1984) 327–334.
[40] E. Kostenidou, R. Pathak, S. Pandis, An algorithm for the calculation of secondary organic aerosol density combining AMS and SMPS data, Aerosol Science and Technology 41 (2007) 1002–1010.
[41] J.H. Seinfeld, S.N. Pandis, Atmospheric Chemistry and Physics, John Wiley & Sons, New York, 1998.
[42] S.M. Aschmann, J. Arey, R. Atkinson, OH radical formation from the gas-phase reactions of O_3 with a series of terpenes, Atmospheric Environment 36 (2002) 4347–4355.
[43] ICRP, Human respiratory tract model for radiological protection, in: Annals of the ICRP publication 66, International Commission of Radiological Protection, 1994.
[44] G. Oberdörster, Toxicology of ultrafine particles: *in vivo* studies, Philosophical Transactions of the Royal Society A: Mathematical, Physical and Engineering Sciences 358 (2000) 2719–2740.
[45] K. Donaldson, X.Y. Li, W. MacNee, Ultrafine (nanometre) particle mediated lung injury, Journal of Aerosol Science 29 (1998) 553–560.
[46] G. Oberdörster, Significance of particle parameters in the evaluation of exposure-dose–response relationships of inhaled particles, Inhalation Toxicology 8 (1996) 73–89.
[47] X.Y. Li, P.S. Gilmour, K. Donaldson, W. MacNee, Free radical activity and proinflammatory effects of particulate air pollution (PM10) *in vivo* and *in vitro*, Thorax 51 (1996) 1216–1222.
[48] C.A. Pope III, R.T. Burnett, G.D. Thurston, M.J. Thun, E.E. Calle, D. Krewski, J.J. Godleski, Cardiovascular mortality and long-term exposure to particulate air pollution: epidemiological evidence of general pathophysiological pathways of disease, Circulation 109 (2004) 71–77.
[49] G. Oberdörster, E. Oberdörster, J. Oberdörster, Nanotoxicology: an emerging discipline evolving from studies of ultrafine particles, Environmental Health Perspectives 113 (2005) 823–839.
[50] W.C. Hinds, Aerosol Technology: Properties, Behavior and Measurement of Airborne Particles, second ed., Wiley Interscience, John Wiley & Sons, Inc., New York, 1999.
[51] D.D. Hunter, R.D. Dey, Identification and neuropeptide content of trigeminal neurons innervating the rat nasal epithelium, Neuroscience 83 (1998) 591–599.
[52] G. Oberdörster, Z. Sharp, V. Atudorei, A. Elder, R. Gelein, W. Kreyling, C. Cox, Translocation of inhaled ultrafine particles to the brain, Inhalation Toxicology 16 (2004) 437–445.
[53] D.D. Hunter, B.J. Undem, Identification and substance P content of vagal afferent neurons innervating the epithelium of the guinea pig trachea, American Journal of Respiratory and Critical Care Medicine 159 (1999) 1943.
[54] D. Bodian, H.A. Howe, The rate of progression of poliomyelitis virus in nerves, Bulletin of the Johns Hopkins Hospital 69 (1941) 79–85.
[55] E. Oberdörster, Manufactured nanomaterials (Fullerenes, C60) induce oxidative stress in the brain of juvenile largemouth bass, Environmental Health Perspectives 112 (2004) 1058–1062.
[56] J.D. McDonald, M. Doyle-Eisele, M.J. Campen, J.C. Seagrave, T. Holmes, A. Lund, J.D. Surratt, J.H. Seinfeld, A.C. Rohr, E.M. Knipping, Cardiopulmonary response to inhalation of biogenic secondary organic aerosol, Inhalation Toxicology 22 (2010) 253–265.
[57] A. Gaschen, D. Lang, M. Kalberer, M. Savi, T. Geiser, A. Gazdhar, C.-M. Lehr, M. Bur, J. Dommen, U. Baltensperger, M. Geiser, Cellular responses after exposure of lung cell cultures to secondary organic aerosol particles, Environmental Science & Technology 44 (2010) 1424–1430.
[58] M. Jang, A.J. Ghio, G. Cao, Exposure of BEAS-2B cells to secondary organic aerosol coated on magnetic nanoparticles, Chemical Reserach in Toxicology 19 (2006) 1044–1050.